



## Relativistic runaway breakdown in low-frequency radio

Martin Füllekrug,<sup>1</sup> Robert Roussel-Dupré,<sup>2</sup> Eugene M. D. Symbalisty,<sup>3</sup> Olivier Chanrion,<sup>4</sup> Anna Odzimek,<sup>5</sup> Oscar van der Velde,<sup>6</sup> and Torsten Neubert<sup>4</sup>

Received 18 May 2009; revised 23 July 2009; accepted 3 September 2009; published 14 January 2010.

[1] The electromagnetic radiation emitted by an electron avalanche beam resulting from relativistic runaway breakdown within the Earth's atmosphere is investigated. It is found from theoretical modeling with a computer simulation that the electron beam emits electromagnetic radiation which is characterized by consecutive broadband pulses in the low-frequency radio range from  $\sim 10$  to 300 kHz at a distance of  $\sim 800$  km. Experimental evidence for the existence of consecutive broadband pulses is provided by low-frequency radio observations of sprite-producing lightning discharges at a distance of  $\sim 550$  km. The measured broadband pulses occur  $\sim 4$ – $9$  ms after the sprite-producing lightning discharge, they exhibit electromagnetic radiation which mainly spans the frequency range from  $\sim 50$  to 350 kHz, and they exhibit complex waveforms without the typical ionospheric reflection of the first hop sky wave. Two consecutive pulses occur  $\sim 4.5$  ms and  $\sim 3$  ms after the causative lightning discharge and coincide with the sprite luminosity. It is concluded that relativistic runaway breakdown within the Earth's atmosphere can emit broadband electromagnetic pulses and possibly generates sprites. The source location of the broadband pulses can be determined with an interferometric network of wideband low-frequency radio receivers to lend further experimental support to the relativistic runaway breakdown theory.

**Citation:** Füllekrug, M., R. Roussel-Dupré, E. M. D. Symbalisty, O. Chanrion, A. Odzimek, O. van der Velde, and T. Neubert (2010), Relativistic runaway breakdown in low-frequency radio, *J. Geophys. Res.*, 115, A00E09, doi:10.1029/2009JA014468.

### 1. Introduction

[2] The conventional breakdown electric field in the atmosphere needs to exceed  $\sim 10^6$  V/m at sea level to initiate a lightning discharge, but these large electric fields are not observed inside thunderclouds. Balloon measurements of electric fields in thunderclouds suggest that the breakdown electric field is on the order of  $\sim 10^5$  V/m at sea level, i.e., an order of magnitude smaller than the conventional breakdown threshold [Marshall *et al.*, 1995]. This observation is explained with the newly recognized phenomenon of relativistic runaway breakdown within the Earth's atmosphere [e.g., Dwyer *et al.*, 2009; Tierney *et al.*, 2005; Gurevich and Zybin, 2005; Smith *et al.*, 2005; Inan, 2005; Dwyer *et al.*, 2003, and references therein]. It was initially proposed that runaway breakdown may be associ-

ated with transient luminous events above thunderstorms [e.g., Roussel-Dupré *et al.*, 1998; Yukhimuk *et al.*, 1998; Roussel-Dupré and Gurevich, 1996; Bell *et al.*, 1995; Roussel-Dupré *et al.*, 1994; Gurevich *et al.*, 1992, and references therein], denoted sprites, blue jets, and gigantic jets [e.g., Krehbiel *et al.*, 2008; Neubert *et al.*, 2008; Füllekrug *et al.*, 2006; Rakov and Uman, 2003; Su *et al.*, 2003; Pasko *et al.*, 2002; Rodger, 1999; Sentman *et al.*, 1995; Wescott *et al.*, 1995, and references therein], but it is now widely accepted that the majority of sprites are streamer discharges [Liu *et al.*, 2006; Pasko *et al.*, 1997]. Yet, it is not possible to exclude the possibility that sprites occasionally coincide with runaway breakdown. The novel physical mechanism of relativistic runaway breakdown requires any energetic seed particles  $\sim 10^{16}$  eV [Gurevich and Zybin, 2005], e.g., from primary cosmic rays [Dwyer *et al.*, 2009], to initiate a strong relativistic runaway discharge with a nonlinear electron avalanche growth [Gurevich *et al.*, 2004, 2003, 2002]. The runaway breakdown process results in a population of particles with energies as high as tens of MeV which can reside inside the thundercloud, above the thundercloud, or both.

[3] Runaway breakdown inside the thundercloud is initiated by the electric field which develops during collisions between riming graupel particles and ice crystals within the mixed phase region of the thundercloud at  $\sim 5$  km height. About  $\sim 50\%$  of the mass of the atmosphere is located below and above 5 km height such that the energetic radiation from runaway breakdown can be observed from

<sup>1</sup>Centre for Space, Atmospheric and Oceanic Science, Department of Electronic and Electrical Engineering, University of Bath, Bath, UK.

<sup>2</sup>SciTech Solutions, Santa Fe, New Mexico, USA.

<sup>3</sup>Atmospheric, Climate and Environmental Dynamics Group, Earth and Environment Sciences Division, Los Alamos National Laboratory, Los Alamos, New Mexico, USA.

<sup>4</sup>National Space Institute, Technical University of Denmark, Copenhagen, Denmark.

<sup>5</sup>Department of Physics and Astronomy, University of Leicester, Leicester, UK.

<sup>6</sup>Department of Electrical Engineering, Universitat Politècnica de Catalunya, Terrassa, Spain.

the ground [Dwyer *et al.*, 2003] and from space [Smith *et al.*, 2005; Fishman *et al.*, 1994]. Alternatively, it was proposed that runaway breakdown could take place above the thundercloud, supposedly initiated by the electric field produced following a lightning discharge [Inan, 2005; Roussel-Dupré and Gurevich, 1996]. This theory predicts that the lightning electric field accelerates free electrons upward to some MeV of energy producing bursts of terrestrial  $\gamma$  rays resulting from bremsstrahlung radiation of the energetic electrons [Lehtinen *et al.*, 1996]. The energetic electrons propagate along the geomagnetic field lines into near-Earth space where they are trapped in the radiation belt and bounce back and forward between conjugate hemispheres while drifting eastward [Lehtinen *et al.*, 2000]. The recent observations of electron beams on board of satellites [Carlson *et al.*, 2009; Dwyer *et al.*, 2008; Burke *et al.*, 1992] seem to support this prediction. Yet, the proposed theory awaits more solid experimental verification and a number of challenging space missions are now under way to simultaneously detect the electron beam, the energetic X-radiation and  $\gamma$  radiation, and the electromagnetic radiation emitted from the relativistic particles. The Japanese IBUKI satellite was launched on 23 January 2009, while the Russian satellite CHIBIS, the French satellite TARANIS, the Danish payload ASIM and the Japanese payload GLIMS on the International Space Station will be launched in the coming years. The TARANIS payload includes electromagnetic radiation detectors working in the frequency range from DC to 30 MHz to record the electromagnetic radiation of relativistic runaway breakdown [Blanc *et al.*, 2007].

[4] Ground based measurements of the low-frequency electromagnetic radiation from relativistic runaway breakdown do currently not exist, even though high-frequency/very high frequency waveforms of narrow bipolar pulses associated with lightning initiation have been reported by use of radio interferometry [Gurevich *et al.*, 2003] and the FORTE satellite [Tierney *et al.*, 2005, and references therein]. However, the properties of lightning discharges producing terrestrial  $\gamma$  ray flashes have been characterized. For example, it was shown that lightning discharges associated with terrestrial  $\gamma$  ray flashes are amongst the most intense lightning discharges within a given thunderstorm [Inan *et al.*, 2006], are possibly related to intracloud lightning discharges [Stanley *et al.*, 2006], and do not exhibit a lightning continuing current [Cummer *et al.*, 2005]. These results strongly suggest that lightning discharges associated with relativistic runaway breakdown need to be measured with specially designed instruments. The aim of this contribution is to predict the electromagnetic radiation emitted by relativistic runaway breakdown above thunderclouds and to compare the theoretical modeling with experimental measurements.

## 2. Theory

[5] The electromagnetic radiation emitted by relativistic runaway breakdown is calculated with a computer simulation. The simulation begins with the calculation of the electromagnetic field resulting from a lightning discharge and determines subsequently the response of the atmosphere by including particles generated from a parametrized steady

state cosmic ray flux. The dissipation of the deposited electromagnetic energy results in the ionization of neutral molecules and the acceleration of particles, both of which change the original electromagnetic field configuration. This complex interaction between macroscopic electromagnetic fields and microscopic particles is solved in a self-consistent way. The computer simulation allows to predict the temporal evolution of the electromagnetic radiation including the effects of runaway and conventional breakdown. This novel modeling uses Maxwell's equations and thereby extends the previous quasi-electrostatic approximation [Roussel-Dupré *et al.*, 1998]. This step enables the computation of the induction and radiation fields, i.e., electric and magnetic fields, and the inclusion of their effect on the electron and ion populations in a self-consistent way. The novel modeling also allows to use a spatially divergent and temporally varying lightning current anywhere within the simulation volume. This modification enables a simulation of the buildup of charge within a thunderstorm. A momentum equation for the relativistic electrons is used to include the effect of magnetic pinching which is characteristic for relativistic electron beams with a large current.

### 2.1. Electromagnetic Equations

[6] The computer simulation is based on Maxwell's equations

$$\frac{\partial \mathbf{B}}{\partial t} = -\nabla \times \mathbf{E}, \quad \frac{\partial \mathbf{D}}{\partial t} = \nabla \times \mathbf{H} - \mathbf{J}, \quad (1)$$

$$\mathbf{B} = \mu \mathbf{H}, \quad \mathbf{D} = \varepsilon \mathbf{E}, \quad \mathbf{J} = \sigma \mathbf{E} + \mathbf{J}_L, \quad (2)$$

where the electric field  $\mathbf{E}$  includes the charge buildup from the lightning current density  $\mathbf{J}_L$ , the primary electron current, the secondary electron current, the ion current, and the electromagnetic radiation. The permittivity  $\varepsilon$  and the permeability  $\mu$  are set to vacuum values for the atmosphere and measured values for the ground. The atmospheric conductivity  $\sigma$  is defined by either the measured ambient atmospheric conductivity  $\sigma_a$  [Hale *et al.*, 1981], or the electron and ion conductivity  $\sigma_c$ , whichever is larger

$$\sigma = \max(\sigma_a, \sigma_c), \quad (3)$$

$$\sigma_c \mathbf{E} = e(n_p v_p + n_s v_s) \frac{\mathbf{E}}{|\mathbf{E}|} + e(n_- + n_+) \mu_i \mathbf{E}, \quad (4)$$

where  $e$  is the electronic charge. The relativistic runaway breakdown mechanism is characterized by two electron population densities, i.e., the primary (or relativistic) electrons with energies  $>10$  keV ( $n_p$ ) and secondary (or slow) electrons with energies  $<100$  eV ( $n_s$ ) which propagate with different drift velocities ( $v_p$  and  $v_s$ ) through the Earth's atmosphere. The formulation for the electron and ion conductivity  $\sigma_c$  assumes that the electrons and negative ions ( $n_-$ ) are moving antiparallel to the electric field and that the positive ions ( $n_+$ ) are moving parallel to the electric field. It

is also assumed that the ions are singly ionized and possess a mobility of [Roble and Tzur, 1986]

$$\mu_i = \mu_r \frac{\rho_0}{\rho}, \quad (5)$$

$$\mu_r = 2.27 \times 10^{-4} \text{ m}^2 \text{V}^{-1} \text{s}^{-1}, \quad \rho_0 = 1.23 \text{ kg m}^{-3}, \quad (6)$$

where  $\rho$  describes the atmospheric density variation with height according to a standard atmospheric model. The computer simulation models the increase of the air conductivity associated with lightning related discharge processes, while the electrical ground conductivity is set to a constant measured value. Maxwell's equations are solved with a finite difference time domain (FDTD) technique [Taflove, 1995]. The current densities in Maxwell's equations are determined by solving for the electron and ion densities and for their respective drift velocities or mobilities by use of the electron and ion continuity equations and the primary electron momentum equation.

## 2.2. Electron and Ion Continuity Equations and Primary Electron Momentum Equation

[7] The temporal evolution of the relativistic (or primary) and the slow (or secondary) electron densities ( $n_p$  and  $n_s$ ) and the negative and positive ion densities ( $n_-$  and  $n_+$ ) is described by the electron and ion continuity equations, and the primary electron momentum equation

$$\frac{\partial n_p}{\partial t} = -\nabla \cdot n_p \mathbf{v}_p + R_p n_p + F_c / \lambda_{\text{mfp}} \quad (7)$$

$$\frac{\partial n_s}{\partial t} = -\nabla \cdot n_s \mathbf{v}_s + R_s n_p + \nu_i n_s - \alpha_3 n_s - \alpha_r n_+ n_s \quad (8)$$

$$\frac{\partial n_-}{\partial t} = -\nabla \cdot n_- \mathbf{v}_- + \alpha_3 n_s - \alpha_i n_+ n_- \quad (9)$$

$$\frac{\partial n_+}{\partial t} = -\nabla \cdot n_+ \mathbf{v}_+ + R_p n_p + R_s n_p + \nu_i n_s - \alpha_i n_+ n_- - \alpha_r n_+ n_s \quad (10)$$

$$\mathbf{S} = m_\gamma n_p \mathbf{v}_p \quad (11)$$

$$\frac{\partial \mathbf{S}}{\partial t} = -\nabla \cdot \mathbf{S} \mathbf{v}_p - e n_p (\mathbf{E} + \mathbf{v}_p \times \mathbf{B}) - \nu \mathbf{S}. \quad (12)$$

The velocity for relativistic (or primary) electrons  $\mathbf{v}_p$  is computed from fits to Boltzmann's equation for avalanche processes. The source terms for the relativistic electrons include the avalanche rate  $R_p$  above the threshold for a runaway avalanche and the energy loss rate below the threshold. Another source term is the parametrized steady state flux of cosmic ray produced high-energy electrons  $F_c$  with a mean free path length of  $\lambda_{\text{mfp}}$  at a height of  $\sim 15$  km. The velocity for slow (or secondary) electrons  $\mathbf{v}_s$  is

computed from fits to swarm data. The source terms for the slow electrons include the production rate of slow electrons which is expressed in the frame of the beam by  $R_s = \frac{\varepsilon_p}{\varepsilon_i} R_p$  [Roussel-Dupré and Gurevich, 1996] by use of the mean primary electron energy  $\varepsilon_p$ , which is balanced against the energy loss per ion pair produced in air  $\varepsilon_i = 34$  eV. Thus, the ratio  $\varepsilon_p/\varepsilon_i$  describes the number of secondary particles produced per primary electron. This ratio is multiplied by the number of primary particles lost/produced per unit time to get the total number of secondary particles per unit time. Another source term for the slow electrons is the avalanche rate  $\nu_i$  which includes the ionization rate minus the dissociative attachment rate. The loss terms for the slow electrons include the three-body attachment rate  $\alpha_3$  and the radiative recombination rate  $\alpha_r$ . The velocity for negative ions  $\mathbf{v}_-$  is computed from listed mobilities. The sink terms for negative ions include the three-body attachment rate  $\alpha_3$  and the ion-ion recombination rate  $\alpha_i$ . The velocity for positive ions  $\mathbf{v}_+$  is computed from listed mobilities. The source terms for positive ions include the avalanche rate for relativistic electrons  $R_p$ , the production rate of slow electrons  $R_s$ , and the avalanche rate for slow electrons  $\nu_i$ . The sink terms for positive ions include the ion-ion recombination rate  $\alpha_i$  and the radiative recombination rate  $\alpha_r$ . The required numerical constants are well documented in the scientific literature [Roussel-Dupré et al., 1998; Ali, 1986; Huxley and Crompton, 1974], e.g., the avalanche rates are known with an accuracy of  $\sim 10$ – $20\%$  [Coleman and Dwyer, 2006].

[8] The relativistic electron momentum flux  $\mathbf{S}$  is characterized by the relativistic mass of the electron  $m_\gamma$ , the relativistic electron density  $n_p$ , and the velocity vector  $\mathbf{v}_p$  of the relativistic electrons which drift according to the electric field force and the Lorentz force imposed by the self-consistent magnetic field. The relativistic electrons are subject to scattering within the Earth's atmosphere which is described by the associated atmospheric scattering rate  $\nu$ . Note that an equation for the slow electron momentum is not yet included in the computer simulation because the drift velocity is specified by swarm measurements as a function of electric field strength. A transient, multimaterial, compressible, fluid dynamics code (CAVEAT) developed at Los Alamos [Addessio et al., 1992] was adapted to solve the electromagnetic equations and their effect on the electron and ion populations on a computational cylindrical grid with a horizontal radius of 36 km, a vertical height of 90 km, and a spatial resolution of 300 m  $\times$  300 m within the simulation volume.

## 2.3. Electromagnetic Radiation

[9] The far field electromagnetic radiation produced by current sources within the simulation volume can be calculated from the near field FDTD solution of Maxwell's equations [Taflove, 1995]. In this technique, the radiated E and H fields are computed by the Maxwell solver. The electromagnetic field components which are tangential to a virtual surface which encloses the entire current system are weighted by the free space Green's function and subsequently integrated to yield the far field electromagnetic radiation. The near field virtual surface can be taken along the boundary of the simulation volume independent of the shape of the electrical current geometry within. The surface

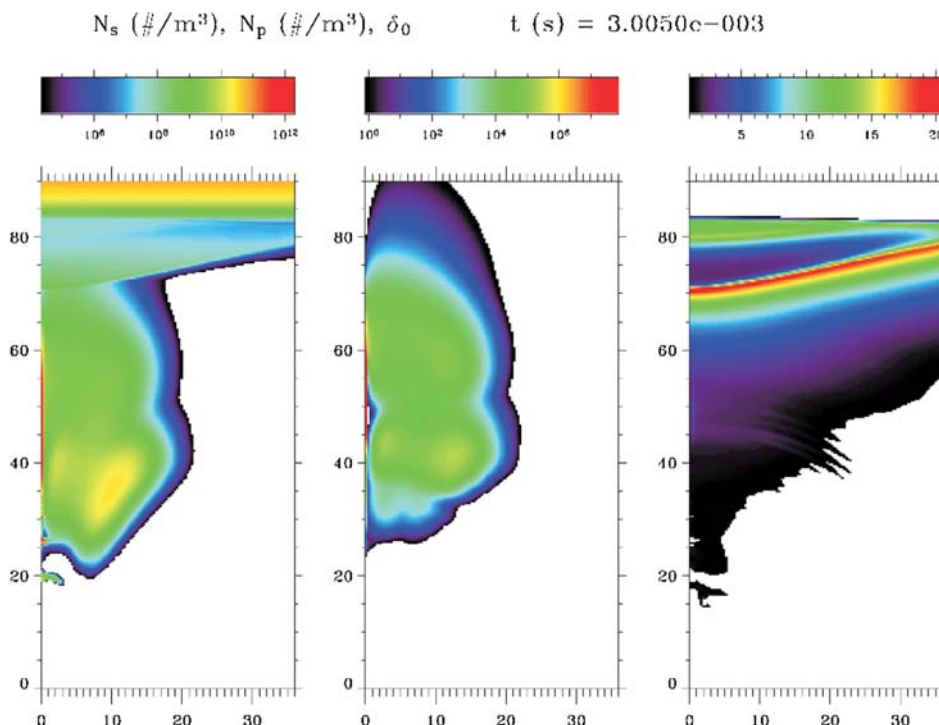


**Figure 1.** Theoretical modeling of relativistic runaway breakdown with a computer simulation at 3 ms after the causative lightning discharge. The lightning discharge causes (right) an electric field above the thundercloud which exceeds the relativistic runaway breakdown threshold. The lightning discharge causes subsequently a population of (middle) relativistic, or primary, electrons and (left) slow, or secondary, electrons.

equivalence theorem provides thereby a convenient methodology for calculating the far field electromagnetic radiation directly from the simulations [Taflove, 1995].

#### 2.4. Simulation

[10] The aim of the computer simulations discussed here is a first attempt to understand theoretically the electromagnetic radiation emitted by an electron beam initiated by the relativistic runaway breakdown process. The initial lightning discharge causes an electric field in the Earth's atmosphere according to the quasi-electrostatic approximation. This process is simulated by introducing the opposite signed charge at the altitude where the cloud charging mechanism initially deposited the charge. Two opposite charge layers are injected into the simulation volume with an exponentially decaying pulse lasting for  $t \approx 2$  ms to simulate the intracloud discharge [Roussel-Dupr e et al., 1998]. In this time a charge of +100 C was deposited at an altitude of 8 km and a charge of -100 C was deposited at an altitude of 15 km over an ellipsoid with a maximum radial diameter of 6 km and a maximum thickness of 1 km. This intracloud discharge would have a charge moment of approximately 700 C · km. Smaller lightning charge moments would scale down the predicted electromagnetic radiation throughout the simulation while qualitatively describing the same physics since the energetic seed particles could still initiate relativistic breakdown process with much smaller lightning charge moments present inside the thundercloud.

[11] The interaction between the macroscopic electromagnetic fields generated by the initial lightning discharge and

the microscopic particles is solved in a self consistent way which results in a complex electromagnetic energy dissipation pattern. After  $\sim 0.5$  ms into the simulation the electric field begins to exceed the threshold for runaway breakdown above an altitude of  $\sim 70$  km. This overvoltage  $\delta_0$ , defined as the ratio of the electric field to the threshold field necessary to initiate runaway breakdown, grows in spatial extent and in magnitude as time proceeds. At 1.0 ms the threshold for conventional breakdown is exceeded over a region  $\sim 4$  km thick and  $\sim 30$  km in diameter. Conventional breakdown develops in this region and leads to an enhanced secondary electron population. The overvoltage continues to grow to  $\delta_0 = 20$  until sufficient conductivity develops to eliminate the electric field over a sizable region  $\sim 2$  km thick and  $\sim 20$  km in diameter. At  $\sim 2.9$  ms into the simulation the field is overvolted over a large spatial range from  $\sim 40$  km to  $\sim 85$  km altitude and from  $\sim 20$  km to  $\sim 30$  km altitude. At this stage a runaway discharge develops near the cloud top at  $\sim 17$  km and it propagates out of the top of the simulation volume. Roughly  $\sim 0.5$  C of primary electrons exit the simulation volume and a column of secondary electrons forms from  $\sim 48$  to 85 km with an electron density of  $\sim 10^{12} \text{ m}^{-3}$  which persists until the end of the simulation at  $\sim 8$  ms.

[12] A snapshot at  $\sim 3$  ms into the simulation shows the differences in the spatial distribution of the overvoltage area, the relativistic electron density, and the slow electron density (Figure 1). The distribution of the relativistic electrons gives rise to a vertical current density (Figure 2). The change in the current density results in a displacement

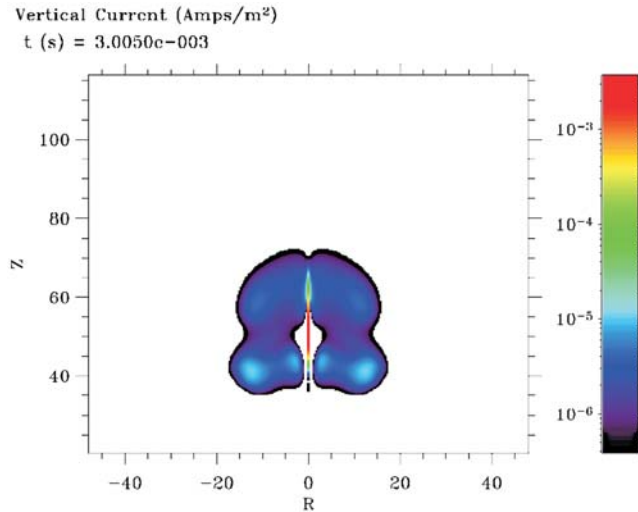


**Figure 2.** The population of relativistic electrons at 3 ms into the computer simulation causes a current density which is particularly high ( $\sim\pm 300$  m) around the center of the causative lightning discharge. The current density changes of the relativistic electron avalanche beam result in a displacement current causing low-frequency electromagnetic radiation. The horizontal (R) and vertical (Z) distances are given in kilometers.

current at  $\sim 3.0$  ms into the simulation and effectively launches an electromagnetic pulse which can be observed at a distance of  $\sim 800$  km away on the ground (Figure 3). The second pulse at  $\sim 5.8$  ms corresponds to a discharge below  $\sim 20$  km where the electric field exceeds the conventional breakdown threshold. The third pulse at  $\sim 6.4$  ms into the simulation corresponds to another runaway breakdown pulse which originates at the cloud top. It is interesting to note that consecutive discharge processes are still ongoing even after the deposition of electromagnetic energy by the causative lightning discharge has finished. This surprising effect is caused by the complex interaction between the macroscopic electromagnetic field reconfiguration and the spatial distribution of the microscopic particle populations which are always self consistent throughout the entire simulation. For example, the runaway electrons which exit at the top of the simulation volume result in a localized electromagnetic field enhancement in the lower portion of the simulation volume.

[13] The consecutive broadband pulses exhibit a duration  $\sim 230 \mu\text{s}$  which is determined by the propagation of the relativistic particles through the atmosphere with a velocity near the speed of light and the time required to relax the field in the upper atmosphere by the remaining slow electrons. The consecutive broadband pulses exhibit an apparent cutoff at a frequency of  $\sim 300$  kHz in the spectrogram (Figure 4). This cutoff results from the limited spatial resolution within the simulation volume. The fastest rate of the current density change caused by runaway breakdown would contribute to the spectrum of the broadband electromagnetic radiation pulse at a frequency of  $\sim 100$  kHz. Yet, the computational resources do not provide the spatial resolution needed to model this high-frequency content accurately. An increase of the grid resolution by a factor

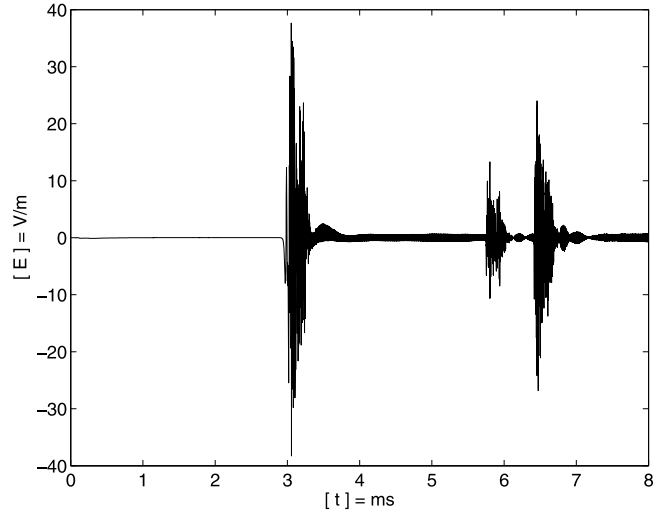


**Figure 3.** The parent lightning discharge occurs at 0 ms (not shown). Two consecutive broadband pulses of low-frequency electromagnetic radiation at  $\sim 3.0$  ms and  $\sim 6.4$  ms into the simulation result from the displacement current of current density changes caused by the relativistic electron avalanche beam. The consecutive pulse at  $\sim 5.8$  ms into the simulation corresponds to a discharge below  $\sim 20$  km where the electric field exceeds the conventional breakdown threshold.

of 4 would increase the run time by a factor of 16 and parallel processing needs to be invoked for a reasonable computation time. An additional complication arises from the highly conducting surfaces near the upper and the lower boundary of the simulation volume, i.e., the ionosphere and

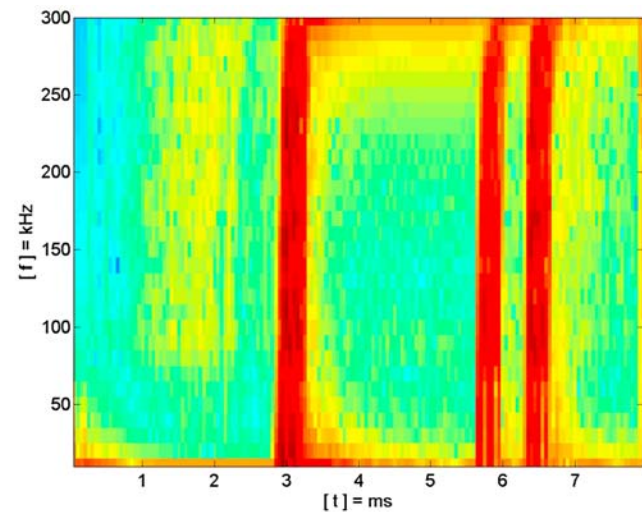


**Figure 4.** The parent lightning discharge occurs at 0 ms (not shown). The spectrogram of low-frequency electromagnetic radiation caused by the relativistic electron avalanche beam exhibits consecutive broadband pulses at  $\sim 3.0$  ms and  $\sim 6.4$  ms which span a frequency range from  $\sim 10$  to 300 kHz. The second pulse corresponds to a discharge below  $\sim 20$  km where the electric field exceeds the conventional breakdown threshold (compare to Figure 3).

the ground. The reflections from these surfaces are embedded in the signals but at delay times corresponding to the travel time to the reflecting boundaries and then to the near field virtual surface used for the far field calculations. The direct and the reflected pulse are separated by  $\sim 150$ – $170 \mu\text{s}$  and they can be distinguished in each of the modeled broadband pulses. At a distance of  $\sim 800$  km on the ground, the reflected pulses would overlap with the direct pulses and result in a complex pattern of the consecutive pulses as observed in the experimental measurements.

### 3. Measurements

[14] In the afternoon of 30 August 2008, intense thunderstorm activity over the Bay of Biscay and northern Spain developed into a mesoscale convective system which propagated northward over France during the night. This electrical storm produced a significant amount of lightning discharges in the evening and in particular many positive lightning discharges during the late night and in the early morning hours of 31 August. Optical camera systems observed the area above the mesoscale convective system from the Pic du Midi in the French Pyrenées and from Sant Vicenç de Castellet in northeastern Spain. Low-frequency radio measurements were installed near Bath in Southwest England, UK. The radio recordings started around 0015 UTC on 31 August and continued until  $\sim 0400$  UTC. During this time interval, the optical camera systems in southern France and northeastern Spain reported the simultaneous observation of numerous sprites.

#### 3.1. Mesoscale Convective System

[15] The weather situation on 30 August 2008 was a classical constellation for summer thunderstorms to occur over the Bay of Biscay and northern Spain with the possibility to evolve subsequently into a mesoscale convective system. A plume of warm and humid air formed in Spain and moved northward while converging over northern Spain and southwestern France near a low-pressure area. A trough with an arrival of colder air at the 500 hPa level destabilized the air mass. The instability developed a convective available potential energy of more than  $\sim 1000$  J/kg with a vertical wind shear vector of  $\sim 15$  m/s over a  $\sim 0$ – $6$  km height range, ultimately organizing the thunderstorm activity into a mesoscale convective system. The mesoscale convective system reaches a cloud canopy measuring  $\sim 400$  km in the longest dimension as inferred from infrared satellite imagery. The radar images show that the mesoscale convective system exhibits numerous convective cores at  $\sim 2200$  UTC which are poorly organized. An area of light and stratiform precipitation begins to form at the southern side of the mesoscale convective system after  $\sim 2300$  UTC which trails two large clustered convective cores. The mesoscale convective system keeps growing but loses its round contours and brightness on the infrared satellite images after  $\sim 2300$  UTC. This temporal evolution is characteristic for sprite-producing thunderstorm systems in France [Soula *et al.*, 2009]. Two distinct regions of stratiform precipitation behind each of the two clustered convective cores can be distinguished at  $\sim 0200$  UTC on 31 August 2008, which are the areas of the sprite occurrences. The mesoscale convective system propagates over central France northward during the night and

decays in the late morning hours of 31 August when reaching the United Kingdom.

#### 3.2. Lightning Activity

[16] The lightning activity is reported by the French lightning detection network Météorage which covers south-western Europe and the western Mediterranean Sea. The radio detection system reports cloud to ground lightning discharges with a detection efficiency of  $\sim 90\%$ , a peak current accuracy of  $\sim 5\%$ , a location accuracy  $< 4$  km, and a timing accuracy  $< 1$  ms [Mika *et al.*, 2005]. The mesoscale convective system which developed over the Bay of Biscay and northern Spain migrates northward over western France in the afternoon and starts to produce significant lightning activity around  $\sim 1500$ – $1700$  UTC on 30 August. The hourly rate of negative lightning discharges peaks between  $\sim 2200$  and  $\sim 2300$  UTC with an average lightning rate of  $\sim 41.4$  events per minute. The hourly rate of positive lightning discharges peaks between  $\sim 2300$  and  $\sim 0000$  UTC with an average lightning rate of  $\sim 3.6$  events per minute which slightly drops to an average lightning rate of  $\sim 3.0$  events per minute until the morning hours  $\sim 0400$  UTC of 31 August. The most intense positive lightning discharges are observed from  $\sim 0000$  to  $\sim 0300$  UTC when the mesoscale convective system produces numerous sprites. The lightning activity decays away together with the mesoscale convective system in the late morning hours  $\sim 0900$ – $1000$  UTC of 31 August.

#### 3.3. Optical Sprite Observations

[17] The sprites above the mesoscale convective system are observed with an optical camera system located at an altitude of 2877 m on the top of Pic du Midi ( $42.93^\circ\text{N}$ ,  $0.14^\circ\text{E}$ ) in the French Pyrenées [Chanrion *et al.*, 2007]. The system consists of two low-light, high-resolution charge-coupled device (CCD) cameras and one photometer. One camera is equipped with a 50 mm, f 0.95 lens with a field of view of  $10^\circ$ . The other camera and the photometer are equipped with a 16 mm, f 1.40 lens with a field of view of  $31^\circ$ . The exposure time for one image of both CCD cameras is 40 ms. The sampling rate of the photometer is 20 kHz with a timing accuracy of  $\sim 50 \mu\text{s}$ . The system is synchronized to UTC with a Global Positioning Satellite (GPS) receiver with an absolute timing accuracy  $< 1$  ms. Special events of interest are detected by an automated trigger software and the observed image sequences are saved to disk with a lossless data compression algorithm to minimize the digital storage media requirements. The entire system is mounted on a pan-tilt unit. It is possible to remotely control the pan-tilt unit over a wireless Internet connection to track sprite-producing storms interactively with a group of scientists [Neubert *et al.*, 2005]. Another sprite observing camera is installed in Sant Vicenç de Castellet ( $41.67^\circ\text{N}$ ,  $1.86^\circ\text{E}$ ), i.e., a Watec 902H2 equipped with a 12 mm, f 0.8 lens with a field of view of  $31^\circ$  and an exposure time of 20 ms. The camera system is connected to a laptop computer via a KIWI-OSD global positioning system (GPS) time inserter. An UFOCapture software is used to trigger recordings of video sequences with sprite occurrences.

#### 3.4. Low-Frequency Radio

[18] A wideband digital low-frequency radio receiver was installed near Bath in Southwest England of the United

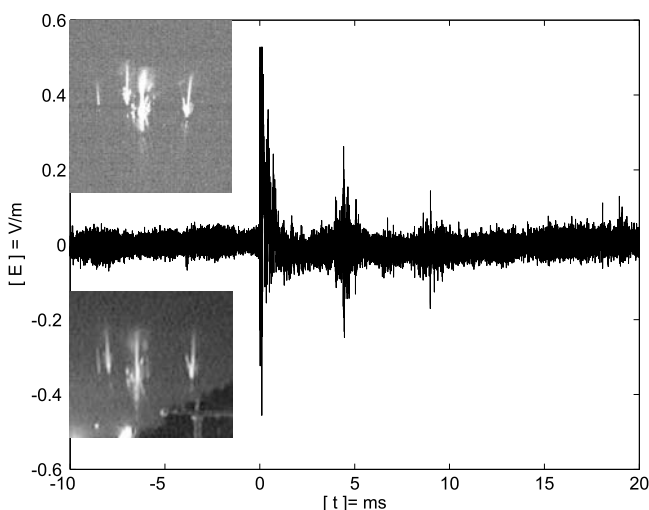


**Figure 5.** Two consecutive broadband pulses of low-frequency electromagnetic radiation at  $\sim 4.5$  ms and  $\sim 9.0$  ms following a sprite-producing lightning discharge at  $\sim 0$  ms. The low-frequency radio waves are measured near Bath in the United Kingdom ( $51.3^{\circ}\text{N}$ ,  $2.3^{\circ}\text{W}$ ),  $\sim 571$  km away from the sprite-producing lightning discharge in France ( $46.5^{\circ}\text{N}$ ,  $0.5^{\circ}\text{E}$ ). The inset images show the sprite as observed by the optical camera systems at Pic du Midi (top image) and San Vicenç de Castellet (bottom image).

Kingdom ( $51.3^{\circ}\text{N}$ ,  $2.3^{\circ}\text{W}$ ) to record the electromagnetic radiation of the lightning discharges within the mesoscale convective system in the early morning hours from 0015 to 0400 UTC on 31 August. The measurement instrument recorded the electrical signal from a capacitive probe with a sampling frequency of 1 MHz and an effective bandwidth from  $\sim 4$  Hz to  $\sim 400$  kHz with an amplitude resolution of  $\sim 35$   $\mu\text{V/m}$ , and a timing accuracy of  $\sim 12$  ns provided by a Global Positioning Satellite (GPS) disciplined frequency standard. Time series of  $\pm 1$  s length around the occurrence times of the nearest positive lightning discharges preceding the sprites were extracted from the digital data and stored for subsequent processing.

[19] For example, a positive lightning discharge occurs near Saint-Julien-l'Ars in France ( $46.54^{\circ}\text{N}$ ,  $0.48^{\circ}\text{E}$ ) on 31 August at 0152:59.524482 UTC. The lightning discharge launches an electromagnetic wave which is recorded  $\sim 571$  km away by the low-frequency radio receiver near Bath (Figure 5). The key time at 0 ms corresponds to the expected arrival time of the electromagnetic wave of the lightning discharge after correction for the time delay introduced by the wave propagation from the source location to the receiver by use of the speed of light. The speed of light is used for correction since the majority of the radio frequencies observed here propagate at or near the speed of light within the Earth's atmosphere. The lightning pulse at 0 ms exhibits a substructure of two consecutive pulses with a time delay of  $\sim 100$   $\mu\text{s}$  which results from the ionospheric reflection of the first hop sky wave. The positive lightning discharge initiates a sprite  $\sim 4.5$  ms after the positive lightning discharge (inset images in Figure 5).

[20] In addition to the lightning pulse at  $\sim 0$  ms, two consecutive pulses of electromagnetic radiation are recorded with a time delay of  $\sim 4.5$  ms and  $\sim 9.0$  ms. Both pulses do

not exhibit the ionospheric reflection from the first hop sky wave which is indicative of a different source altitude and/or a different physical generation mechanism. The frequency content of the consecutive pulses can be determined with a spectrogram which is calculated with a time resolution of 1 ms and a frequency resolution of 1 kHz. The spectrogram exhibits the radio signals of amplitude modulated longwave transmitters (horizontal lines), e.g., the United Kingdom radio clock at 60 kHz (the former Rugby MSF signal, now transmitted from Anthorn), France Inter at 162 kHz, Europe 1 at 183 kHz, and BBC radio 4 at 198 kHz (Figure 6). The spectrogram also shows the broadband pulses at  $\sim 4.5$  ms and  $\sim 9.0$  ms (vertical lines) which mainly span the frequency range from  $\sim 50$  to 350 kHz. An interesting consequence of this observation is that the consecutive pulses would have been missed by narrowband lightning detectors. For example, the Arrival Time Difference (ATD) lightning detection network of the British Meteorological Office reported the first pulse from the positive lightning discharge but not the two consecutive pulses (A. B. Bennett, personal communication, 2008). The upper trace of the spectrogram shows the temporal evolution of the sprite luminosity as recorded by the photometer of the optical camera system. The key time at 0 ms corresponds to the expected arrival time of the lightning discharge photons after correction for the time delay introduced by the propagation from the lightning location to the optical camera system by use of the speed of light. The first consecutive pulse at  $\sim 4.5$  ms coincides with the maximum of the sprite luminosity which is indicative of a physical connection between the broadband low-frequency radio signature and the sprite.

[21] Another positive lightning discharge occurs near Châtelleraut in France ( $46.87^{\circ}\text{N}$ ,  $0.55^{\circ}\text{E}$ ) on 31 August at 0218:26.265226 UTC,  $\sim 540$  km away from the low-frequency radio receiver near Bath (Figure 7). The lightning

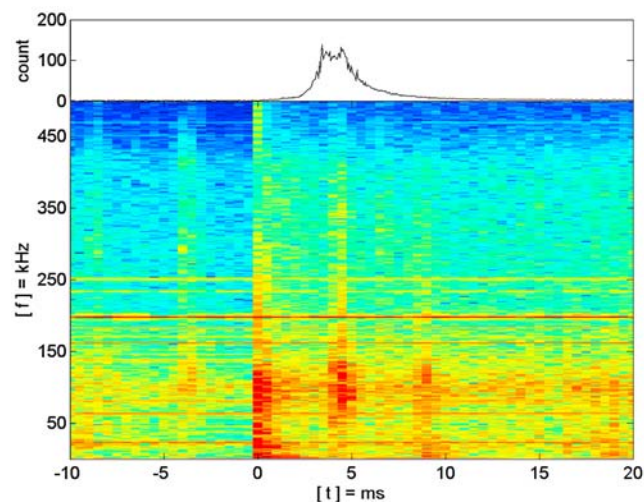


**Figure 6.** (top) The photometric recordings of the optical camera system. The maximum sprite luminosity coincides with the first consecutive pulse at  $\sim 4.5$  ms. (bottom) Spectrogram of two consecutive broadband pulses of low-frequency electromagnetic radiation following a sprite-producing lightning discharge (compare to Figure 5). The measured broadband pulses mainly span a frequency range from  $\sim 50$  to 350 kHz.

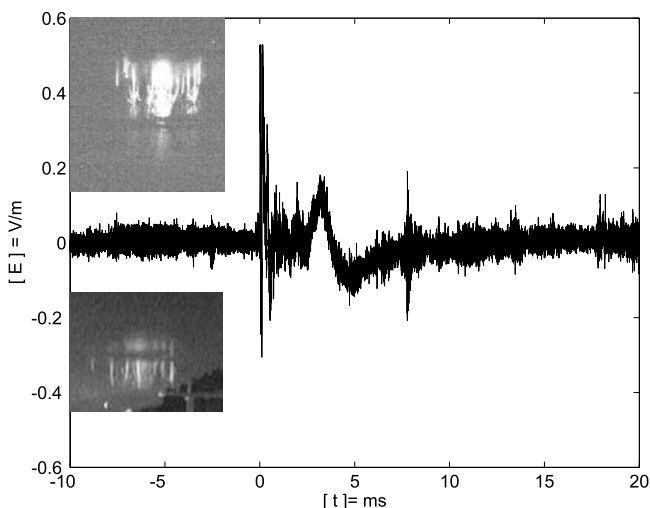


**Figure 7.** One consecutive broadband pulse of low-frequency electromagnetic radiation at  $\sim 8.0$  ms follows a sprite-producing lightning discharge at  $\sim 0$  ms. The low-frequency radio waves are measured near Bath in the United Kingdom ( $51.3^{\circ}\text{N}$ ,  $2.3^{\circ}\text{W}$ ),  $\sim 540$  km away from the lightning discharge in France ( $47.0^{\circ}\text{N}$ ,  $0.5^{\circ}\text{E}$ ). The narrowband pulse at  $\sim 3$  ms is the electromagnetic radiation from the sprite itself. The inset images show the particularly bright sprite as observed by the optical camera systems at Pic du Midi (top image) and San Vicenç de Castellet (bottom image).

pulse at  $\sim 0$  ms exhibits a substructure of two consecutive pulses from the ionospheric reflection of the first hop sky wave. In addition to the lightning pulse, two consecutive pulses of electromagnetic radiation are recorded with a time delay of  $\sim 3$  ms and  $\sim 8$  ms. The narrowband pulse at  $\sim 3$  ms spans a frequency range from  $\sim 100$  to  $300$  Hz and it results from the electromagnetic radiation of the sprite itself [Füllekrug et al., 2001; Cummer et al., 1998; Reising et al., 1996; Boccippio et al., 1995; Burke and Jones, 1992; Farrell and Desch, 1992]. Only  $\sim 20\%$  of all sprites exhibit such type of signature [Füllekrug and Reising, 1998] which scales with the luminosity of the sprite [Reising et al., 1999] and which is explained by conventional breakdown of the mesosphere [Cummer and Füllekrug, 2001; Pasko et al., 1998]. The sprite observed by the optical camera system was particularly bright (inset images in Figure 7). The second consecutive pulse at  $\sim 8$  ms is similar to the two consecutive pulses observed after 0152:59.524482 UTC (compare to Figure 5); that is, the pulse does not exhibit the ionospheric reflection from the first hop sky wave. The frequency content of this pulse is similar to the two consecutive pulses  $\sim 50$ – $350$  kHz (compare to Figure 6), but the pulse exhibits some intensity below  $\sim 50$  kHz (Figure 8). The upper trace of the spectrogram shows the photometric recordings of the sprite luminosity which coincides with the electromagnetic radiation from the sprite itself at  $\sim 3$  ms.

#### 4. Summary

[22] The theoretical modeling of relativistic runaway breakdown caused by the electric field of lightning discharges predicts consecutive pulses of broadband electromagnetic signatures in the low-frequency radio range from

$\sim 10$  to  $300$  kHz. Broadband pulses in the low-frequency radio range from  $\sim 50$  to  $350$  kHz are observed  $\sim 4$ – $9$  ms after lightning discharges which produce sprites. The sprite luminosity coincides in time with one of the broadband pulses and with one narrowband pulse from the electromagnetic radiation of the sprite itself. The bandwidth of the broadband pulses, the coincidence of the broadband pulse with the sprite luminosity, and the complex waveforms of the broadband pulses without the typical ionospheric reflection from the first hop sky wave all indicate a physical generation mechanism which is different from conventional cloud to ground lightning discharges. Conventional cloud to ground discharges would normally exhibit a spectral maximum at  $\sim 10$  kHz which is absent in the observed consecutive pulses. The electromagnetic radiation from horizontal intracloud discharges is quickly attenuated during the propagation within the Earth-ionosphere cavity and is less likely to cause the observed strong consecutive pulses. It is hence not possible to exclude the possibility that relativistic runaway breakdown within the Earth's atmosphere can emit the observed broadband electromagnetic pulses which may occasionally coincide with sprites. An important theoretical investigation lending further support to the relativistic breakdown theory is a better matching of the simulated sequence of consecutive pulses and their amplitudes with the observed consecutive pulses. An important experiment in support of the relativistic runaway breakdown theory is the determination of the source location of the consecutive broadband pulses. Are the radio sources of the broadband pulses located inside the thundercloud, near the thundercloud top, or well above the thundercloud in the stratosphere or the mesosphere? This question can be answered with an interferometric network of wideband low-frequency radio receivers. Another interesting question is if the consecutive broadband pulses from relativistic runaway break-

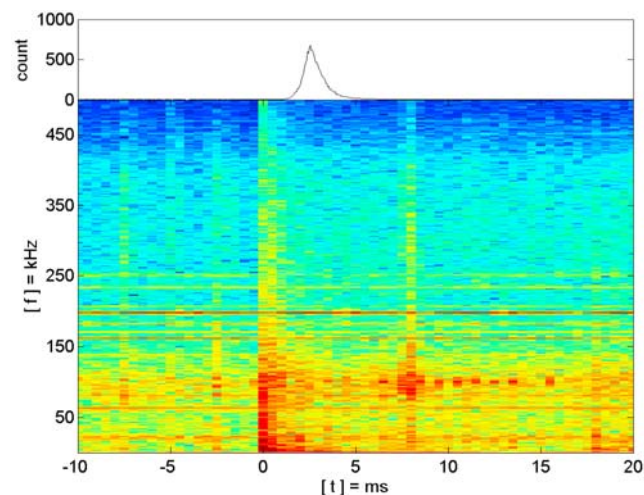


**Figure 8.** (top) The photometric recordings of the optical camera system. The maximum sprite luminosity coincides with the electromagnetic radiation from the sprite at  $\sim 3.0$  ms. (bottom) Spectrogram of one consecutive broadband pulse of low-frequency electromagnetic radiation  $\sim 8.0$  ms following a sprite-producing lightning discharge (compare to Figure 7). The measured broadband pulse mainly spans a frequency range from  $\sim 50$  to  $350$  kHz.

down can be observed from space by radio satellites such as TARANIS [Blanc *et al.*, 2007]. Initial observations indicate that the electromagnetic radiation at  $\sim 100$  kHz is attenuated by  $\sim 40$  dB during the propagation through the ionosphere [Füllekrug *et al.*, 2009]. The experimental results reported here will thereby enable a quantitative estimate of the instrumental sensitivity required on radio satellites to record the electromagnetic signatures of relativistic runaway breakdown from space.

[23] **Acknowledgments.** This work was sponsored by the Science and Technology Facilities Council under grant PP/E0011483/1. The International Space Science Institute (ISSI) kindly supported and hosted the Coupling of Atmospheric Regions with Near-Earth Space team meetings (ISSI 105) which stimulated this work.

[24] Amitava Bhattacharjee thanks the reviewers for their assistance in evaluating this paper.

## References

- Addessio, F., J. Baumgardner, J. Dukowicz, N. Johnson, B. Kashiwa, R. Rauenzahn, and C. Ziemach (1992), CAVEAT: A computer code for fluid dynamics problems with large distortion and internal slip, *Los Alamos Natl. Lab. Rep. LA, 10613-MS-Rev.1*.
- Ali, A. W. (1986), Intense and short pulse electric field (DC and microwave) air breakdown parameters, *NRL Memo. Rep.*, 5815.
- Bell, T., V. Pasko, and U. Inan (1995), Runaway electrons as a source of red sprites in the mesosphere, *Geophys. Res. Lett.*, 22(16), 2127–2130.
- Blanc, E., F. Lefeuvre, R. Roussel-Dupré, and J. Sauvaud (2007), TARANIS: A microsatellite project dedicated to the study of impulsive transfers of energy between the Earth atmosphere, the ionosphere, and the magnetosphere, *Adv. Space Res.*, 40(8), 1268–1275.
- Boccippio, D., E. Williams, S. Heckman, W. Lyons, I. Baker, and R. Boldi (1995), Sprites, ELF transients, and positive ground strokes, *Science*, 269, 1088–1091.
- Burke, C., and D. Jones (1992), An experimental investigation of ELF attenuation rates in the Earth-ionosphere duct, *J. Atmos. Terr. Phys.*, 54, 243–250.
- Burke, W. J., T. L. Aggson, N. C. Maynard, W. R. Hoegy, R. A. Hoffman, R. M. Candy, C. Liebrecht, and E. Rodgers (1992), Effects of a lightning discharge detected by the DE 2 satellite over Hurricane Debbie, *J. Geophys. Res.*, 97, 6359–6367.
- Carlson, B., N. Lehtinen, and U. Inan (2009), Observations of terrestrial gamma-ray flash electrons, in *Coupling of Thunderstorms and Lightning Discharges to Near-Earth Space*, edited by N. B. Crosby, T.-Y. Huang, and M. J. Rycroft, pp. 84–91, Am. Inst. of Phys., Melville, N. Y.
- Chanrion, O., et al. (2007), The EuroSprite2005 observational campaign: An example of training and outreach opportunities for CAL young scientists, *Adv. Geosci.*, 13, 3–9.
- Coleman, L. M., and J. R. Dwyer (2006), Propagation speed of runaway electron avalanches, *Geophys. Res. Lett.*, 33, L11810, doi:10.1029/2006GL025863.
- Cummer, S. A., and M. Füllekrug (2001), Unusually intense continuing current in lightning produces delayed mesospheric breakdown, *Geophys. Res. Lett.*, 28(3), 495–498.
- Cummer, S. A., U. S. Inan, T. F. Bell, and C. P. Barrington-Leigh (1998), ELF radiation produced by electrical currents in sprites, *Geophys. Res. Lett.*, 25(8), 1281–1284.
- Cummer, S. A., Y. Zhai, W. Hu, D. M. Smith, L. I. Lopez, and M. A. Stanley (2005), Measurements and implications of the relationship between lightning and terrestrial gamma ray flashes, *Geophys. Res. Lett.*, 32, L08811, doi:10.1029/2005GL022778.
- Dwyer, J. R., et al. (2003), Energetic radiation produced during rocket-triggered lightning, *Science*, 299, 694–697.
- Dwyer, J. R., B. W. Grefenstette, and D. M. Smith (2008), High-energy electron beams launched into space by thunderstorms, *Geophys. Res. Lett.*, 35, L02815, doi:10.1029/2007GL032430.
- Dwyer, J. R., M. A. Uman, and H. K. Rassoul (2009), Remote measurements of thundercloud electrostatic fields, *J. Geophys. Res.*, 114, D09208, doi:10.1029/2008JD011386.
- Farrell, W., and M. Desch (1992), Cloud-to-stratosphere lightning discharges: A radio emission model, *Geophys. Res. Lett.*, 19(7), 665–668.
- Fishman, G., et al. (1994), Discovery of intense gamma-ray flashes of atmospheric origin, *Science*, 264, 1313–1316.
- Füllekrug, M., and S. C. Reising (1998), Excitation of Earth-ionosphere cavity resonances by sprite-associated lightning flashes, *Geophys. Res. Lett.*, 25(22), 4145–4148.
- Füllekrug, M., D. Moudry, G. Dawes, and D. Sentman (2001), Mesospheric sprite current triangulation, *J. Geophys. Res.*, 106, 20,189–20,194.
- Füllekrug, M., E. A. Mareev, and M. J. Rycroft (Eds.) (2006), *Sprites, Elves and Intense Lightning Discharges*, NATO Sci. Ser., Ser. 2, vol. 225, Springer, Dordrecht, Netherlands.
- Füllekrug, M., M. Parrot, M. Ash, I. Astin, P. Williams, and R. Talhi (2009), Transionospheric attenuation of 100 kHz radio waves inferred from satellite and ground based observations, *Geophys. Res. Lett.*, 36, L06104, doi:10.1029/2008GL036988.
- Gurevich, A., and K. Zybin (2005), Runaway breakdown and the mysteries of lightning, *Phys. Today*, 58(4), 37–43.
- Gurevich, A., G. Milikh, and R. Roussel-Dupré (1992), Runaway electron mechanism of air breakdown and preconditioning during a thunderstorm, *Phys. Lett. A*, 165, 463–468.
- Gurevich, A., L. Duncan, Y. Medvedev, and K. Zybin (2002), Radio emission due to simultaneous effect of runaway breakdown and extensive atmospheric showers, *Phys. Lett. A*, 301, 320–326.
- Gurevich, A., L. Duncan, A. Karashtin, and K. Zybin (2003), Radio emission of lightning initiation, *Phys. Lett. A*, 312, 228–237.
- Gurevich, A., Y. Medvedev, and K. Zybin (2004), Thermal electrons and electric current generated by runaway breakdown effect, *Phys. Lett. A*, 321, 179–184.
- Hale, L. C., C. L. Croskey, and J. D. Mitchell (1981), Measurements of middle-atmosphere electric fields and associated electrical conductivities, *Geophys. Res. Lett.*, 8(8), 927–930.
- Huxley, L., and R. Crompton (1974), *The Diffusion and Drift of Electrons in Gases*, John Wiley, New York.
- Inan, U. (2005), Gamma rays made on Earth, *Science*, 307, 1054–1055.
- Inan, U. S., M. B. Cohen, R. K. Said, D. M. Smith, and L. I. Lopez (2006), Terrestrial gamma ray flashes and lightning discharges, *Geophys. Res. Lett.*, 33, L18802, doi:10.1029/2006GL027085.
- Krehbiel, P., J. Riousset, V. Pasko, R. Thomas, W. Rison, M. Stanley, and H. Edens (2008), Upward electrical discharges from thunderstorms, *Nat. Geosci.*, 1, 233–237.
- Lehtinen, N. G., M. Walt, U. S. Inan, T. F. Bell, and V. P. Pasko (1996),  $\gamma$ -ray emission produced by a relativistic beam of runaway electrons accelerated by quasi-electrostatic thundercloud fields, *Geophys. Res. Lett.*, 23(19), 2645–2648.
- Lehtinen, N. G., U. S. Inan, and T. F. Bell (2000), Trapped energetic electron curtains produced by thunderstorm driven relativistic runaway electrons, *Geophys. Res. Lett.*, 27(8), 1095–1098.
- Liu, N., et al. (2006), Comparison of results from sprite streamer modeling with spectrophotometric measurements by ISUAL instrument on FORMOSAT-2 satellite, *Geophys. Res. Lett.*, 33, L01101, doi:10.1029/2005GL024243.
- Marshall, T., M. McCarthy, and W. Rust (1995), Electric field magnitudes and lightning initiation in thunderstorms, *J. Geophys. Res.*, 100, 7097–7103.
- Mika, A., C. Haldoupis, R. Marshall, T. Neubert, and U. Inan (2005), Subionospheric VLF signatures and their association with sprites observed during EuroSprite2003, *J. Atmos. Sol. Terr. Phys.*, 67, 1580–1597.
- Neubert, T., et al. (2005), Co-ordinated observations of transient luminous events during the EuroSprite2003 campaign, *J. Atmos. Sol. Terr. Phys.*, 67, 807–820.
- Neubert, T., et al. (2008), Recent results from studies of electric discharges in the mesosphere, *Surv. Geophys.*, 29(2), 71–137.
- Pasko, V., U. Inan, T. Bell, and Y. Taranenko (1997), Sprites produced by quasi-electrostatic heating and ionization in the lower ionosphere, *J. Geophys. Res.*, 102, 4529–4561.
- Pasko, V., U. Inan, T. Bell, and S. Reising (1998), Mechanism of ELF radiation from sprites, *Geophys. Res. Lett.*, 25(18), 3493–3496.
- Pasko, V., M. Stanley, J. Mathews, U. Inan, and T. Wood (2002), Electrical discharge from a thundercloud top to the lower ionosphere, *Nature*, 416, 152–154.
- Rakov, V., and M. Uman (2003), *Lightning, Physics and Effects*, Cambridge Univ. Press, Cambridge, U. K.
- Reising, S. C., U. S. Inan, T. F. Bell, and W. A. Lyons (1996), Evidence for continuing currents in sprite-producing cloud-to-ground lightning, *Geophys. Res. Lett.*, 23(24), 3639–3642.
- Reising, S. C., U. S. Inan, and T. F. Bell (1999), ELF spheric energy as a proxy indicator for sprite occurrence, *Geophys. Res. Lett.*, 26(7), 987–990.
- Roble, R., and I. Tzur (1986), The global atmospheric-electrical circuit, in *The Earth's Electrical Environment*, edited by E. Krider and R. Roble, pp. 206–231, Natl. Acad., Washington, D. C.
- Rodger, C. (1999), Red sprites, upward lightning, and VLF perturbations, *Rev. Geophys.*, 37(3), 317–336.
- Roussel-Dupré, R., and A. Gurevich (1996), On runaway breakdown and upward propagating discharges, *J. Geophys. Res.*, 101, 2297–2311.
- Roussel-Dupré, R., A. Gurevich, A. Tunnell, and G. Milikh (1994), Kinetic theory of runaway air breakdown, *Phys. Rev. E*, 49, 2257–2271.

- Roussel-Dupré, R., E. Symbalisy, Y. Taranenko, and V. Yukhimuk (1998), Simulations of high-altitude discharges initiated by runaway breakdown, *J. Atmos. Sol. Terr. Phys.*, *60*, 917–940.
- Sentman, D., E. Wescott, D. Osborne, D. Hampton, and M. Heavner (1995), Preliminary results from the Sprites94 aircraft campaign: 1. Red sprites, *Geophys. Res. Lett.*, *22*(10), 1205–1208.
- Smith, D., L. Lopez, R. Lin, and C. Barrington-Leigh (2005), Terrestrial gamma-ray flashes observed up to 20 MeV, *Science*, *307*, 1085–1088.
- Soula, S., O. van der Velde, J. Montanyà, T. Neubert, O. Chanrion, and M. Ganot (2009), Analysis of thunderstorm and lightning activity associated with sprites observed during the EuroSprite campaigns: Two case studies, *Atmos. Res.*, *91*(2–4), 514–528, doi:10.1016/j.atmosres.2008.06.017.
- Stanley, M. A., X.-M. Shao, D. M. Smith, L. I. Lopez, M. B. Pongratz, J. D. Harlin, M. Stock, and A. Regan (2006), A link between terrestrial gamma-ray flashes and intracloud lightning discharges, *Geophys. Res. Lett.*, *33*, L06803, doi:10.1029/2005GL025537.
- Su, H., R. Su, A. Chen, Y. Wang, W. Hsiao, W. Lai, L. Lee, M. Sato, and H. Fukunishi (2003), Gigantic jets between a thundercloud and the ionosphere, *Nature*, *423*, 974–976.
- Taflove, A. (1995), *Computational Electrodynamics: The Finite Difference Time-Domain Method*, Artech House, Norwood, Mass.
- Tierney, H. E., R. A. Roussel-Dupré, E. M. D. Symbalisy, and W. H. Beasley (2005), Radio frequency emissions from a runaway electron avalanche model compared with intense, transient signals from thunderstorms, *J. Geophys. Res.*, *110*, D12109, doi:10.1029/2004JD005381.
- Wescott, E., D. Sentman, D. Osborne, D. Hampton, and M. Heavner (1995), Preliminary results from the Sprites94 aircraft campaign: 2. Blue jets, *Geophys. Res. Lett.*, *22*(10), 1209–1212.
- Yukhimuk, V., R. A. Roussel-Dupré, E. M. D. Symbalisy, and Y. Taranenko (1998), Optical characteristics of blue jets produced by runaway air breakdown, simulation results, *Geophys. Res. Lett.*, *25*(17), 3289–3292.
- 
- O. Chanrion and T. Neubert, National Space Institute, Technical University of Denmark, DK-2100 Copenhagen, Denmark.
- M. Füllekrug, Centre for Space, Atmospheric and Oceanic Science, Department of Electronic and Electrical Engineering, University of Bath, Bath BA2 7AY, UK. (eesmf@bath.ac.uk)
- A. Odzimek, Department of Physics and Astronomy, University of Leicester, Leicester LE1 7RH, UK.
- R. Roussel-Dupré, SciTech Solutions, 14 Blue Jay Dr., Santa Fe, NM 87506, USA.
- E. M. D. Symbalisy, Atmospheric, Climate and Environmental Dynamics Group, Earth and Environment Sciences Division, Los Alamos National Laboratory, Los Alamos, NM 87545, USA.
- O. van der Velde, Department of Electrical Engineering, Universitat Politècnica de Catalunya, E-08222 Terrassa, Spain.